Earth Planets Space, **62**, 153–165, 2010

Muon tomography: Plans for observations in the Lesser Antilles

Dominique Gibert[1], François Beauducel[1], Yves Déclais[2], Nolwenn Lesparre[1], Jacques Marteau[2], Florence Nicollin[3], and Albert Tarantola[1*]

[1]*Institut de Physique de Globe de Paris, UMR 7154 CNRS/INSU, Université Paris Cité, 4 Place Jussieu, Case 89, 75252 Paris cedex 5, France*
[2]*Institut de Physique Nucléaire de Lyon, UMR 5822 CNRS/IN2P3, Domaine scientifique de la Doua, 4 Rue Enrico Fermi, 69622 Villeurbanne cedex, France*
[3]*Géosciences Rennes, UMR 6118 CNRS/INSU, B15 Campus de Beaulieu, 35042 Rennes cedex, France*

(Received November 23, 2008; Revised June 25, 2009; Accepted July 10, 2009; Online published February 22, 2010)

The application of muon tomography to monitor and image the internal structure of volcanoes in the Lesser Antilles is discussed. Particular focus is directed towards the three volcanoes that fall under the responsibility of the Institut de Physique du Globe of Paris, namely La Montagne Pelée in Martinique, La Soufrière in Guadeloupe, and the Soufrière Hills in Montserrat. The technological criteria for the design of portable muon telescopes are presented in detail for both their mechanical and electronic aspects. The detector matrices are constructed with scintillator strips, and their detection characteristics are discussed. The tomography inversion is presented, and its distinctive characteristics are brie y discussed. Details are given on the implementation of muon tomography experiments on La Soufrière in Guadeloupe.
Key words: Volcanoes, monitoring, tomography, Martinique, Guadeloupe, Montserrat, telescope, muons, cosmic rays.

1. Introduction

Lesser Antilles is a subduction volcanic arc within which a dozen of either potentially or presently active volcanoes are located in populated areas (Fig. 1) (Lindsay *et al*., 2005). These examples are Martinique (La Montagne Pelée), Guadeloupe (La Soufrière), and Montserrat (The Soufrière Hills), whose volcanoes have presented an eruptive activity since the beginning of the 20th century. The last activity of La Montagne Pelée occurred in 1929 (Romer, 1931), i.e., 27 years after the catastrophic 1902 eruption which killed 29,000 people (Lacroix, 1904). In Guadeloupe, La Soufrière had two phreatic eruptive episodes in 1956 (Jolivet, 1958) and 1976–1977 (Le Guern *et al*., 1980; Feuillard *et al*., 1983), and this later event motivated the evacuation of nearly 73,000 persons during a 6-month period. The Soufrière Hills in Montserrat is presently in a magmatic eruption phase which started in 1995 and has since devastated most of the island (Druitt and Kokelaar, 2002).

Because of their societal impacts, these volcanoes are subject to careful monitoring, and fully functional observatories have been installed in their vicinity for this purpose. Besides operating a network of classical techniques, like seismic, chemical, or ground deformation monitoring, these observatories also provide unique privileged places for developing and testing new methods which could ultimately be integrated into the monitoring panoply.

The aim of volcanological monitoring is to evaluate the present state of the volcano within its eruption cycle, estimate its evolution in the near future, and quantify the associated risk for surrounding inhabitants. In practice, various methods and techniques must be carried on, and a number of unknowns still remain in our current body of knowledge of physical and chemical processes that lead to an eruption.

Quantifying an eruption hazard amounts to imaging the volcano interior (structures and plumbing system geometry) and estimating the different source parameters (variations of volume, density, strain, or pressure) associated with uid transports (magma, gas, or water) or physical and chemical evolution of the volcanic materials (e.g., hydrothermal alteration). Geophysical and geochemical techniques used on volcanoes may all lead to estimates of these parameters, sometimes with direct measurements, mostly with modeling and strong hypothesis.

1.1 Volcano monitoring in the Lesser Antilles

Volcanoes in the Lesser Antilles have a very short period of historical data compared to their mean eruption cycle of hundreds of years, and most of the volcanoes had very few observed magmatic eruptions (Lindsay *et al*., 2005). This is a major dif culty in terms of monitoring and hazard assessment since the long-time baselines are not suf ciently constrained. We focus here on the three active volcanoes whose monitoring is under the responsibility of France and where muon tomography is planned in a near future (Fig. 2): Mt. Pelée in Martinique, La Soufrière in Guadeloupe, and Soufrière Hills in Montserrat (co-responsibility with the Seismic Research Centre of Trinidad). These three volca-

*Deceased on December 6, 2009.

doi:10.5047/eps.2009.07.003

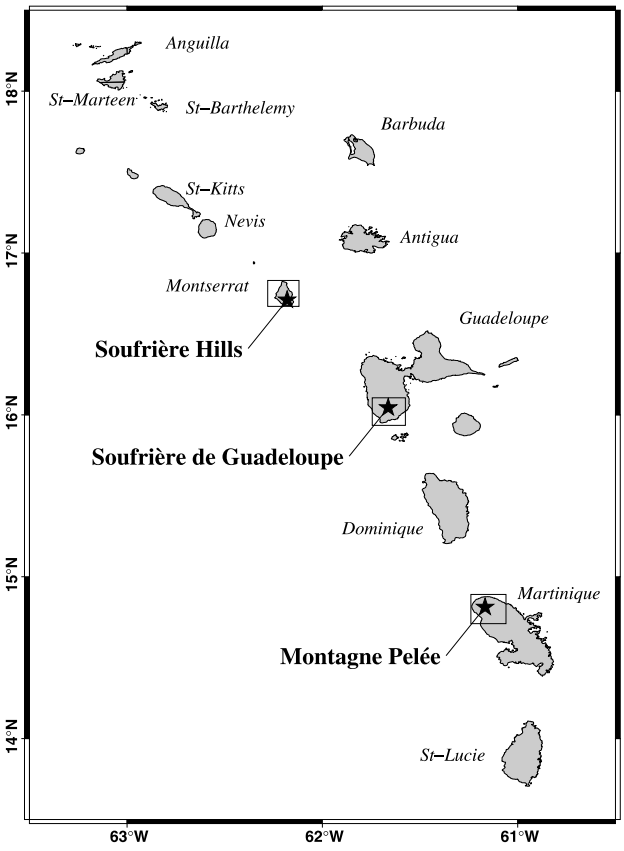

Fig. 1. Location of Lesser Antilles islands and active volcanoes addressed in this paper.

noes are at the present time in three different states: dormant, early unrest activity, and ongoing magmatic eruption, respectively.

La Montagne Pelée (Fig. 2(F)) is presently in a quiet state since the two last magmatic eruptions of 1902 and 1929–1932. The last fumaroles ceased to be active in 1970, and the surface hydrothermal spots currently existing are three low-temperature thermal springs located on the volcano flanks. Seismic volcanic activity is also very weak, with less than 30 events per year (magnitudes lower than 1.7, few kilometers deep), and there is no detectable ground deformation. Permanent survey allows the present volcanic state to be diagnosed with confidence: no significant magmatic activity at depth, and no eruptive phenomena expected in the next years. Consequently, the alert level is maintained at level 1 (i.e., green). Nevertheless, the magma chamber is probably being slowly fed from a deeper supply, but with neither detectable overpressure nor secondary effects, while the shallow hydrothermal system is in a steady state. Current instrumental observations at La Montagne Pelée can be used as a baseline before any eruption precursor signs.

La Soufrière of Guadeloupe (Fig. 2(E)) is in a more serious state. Its last magmatic eruption is estimated to have been 1530 AD (Boudon *et al.*, 2008; Komorowski *et al.*, 2008) and, since then, six phreatic eruptions have occurred: 1690, 1797–1798, 1812, 1836–1837, 1956, and 1976–1977. The last unrest was interpreted as a still-born magmatic eruption by Feuillard *et al.* (1983) (see also Villemant *et al.*, 2005). A renewal of activity started in 1992, and several parameters are currently slowly increasing: intensification of shallow seismicity with long-period events, spatial extension and flux increase of the fumarolic activity at the summit of the volcano, changes in the chemical composition of the gas (sulfur and chlorine), and increases the temperature at several hydrothermal spots. These changes motivated raising the alert level from level 1 (green) to level 2 (yellow). Observations at La Soufrière of Guadeloupe should allow any signs associated with the evolution of the hydrothermal system to be detected, as well as precursors of a possible eruption in the next years, which should likely be a phreatic type. Among the three volcanoes described in this paper, La Soufrière of Guadeloupe is the first volcano where muon tomography is presently being implemented (more details are given in Section 4.1).

The Soufrière Hills (Fig. 2(D)) on-going magmatic eruption started in 1995, after a long period of dormancy since the previous magmatic eruption dated in the 17th century (Lindsay *et al.*, 2005). The current activity pattern leads to alternated periods of rapid or slow lava dome growth, partial or total dome collapses, pyroclastic flows, and ash explosions. These various phenomena have resulted in the total destruction of the southern half of the island, including the capital city Plymouth, which is currently covered by several tens of meters of debris deposits. On June 25, 1997, a large pyroclastic flow killed 19 people and destroyed the island's airport (Baxter *et al.*, 2005). The total volume of magma erupted is estimated to be 9×10^8 m^3 (Elsworth *et al.*, 2008) for a maximum rate of lava dome of 10 m^3 s^{-1} in some periods. Two major dome collapses occurred in 2003 involving approximately 210×10^6 m^3 of material (Herd *et al.*, 2005), and the last one occurred in 2006 with 90×10^6 m^3. Both of these initiated a small tsunami over the Guadeloupe coast (see http://www.mvo.ms for detailed information). Observations at Soufrière Hills provide a unique opportunity in the Lesser Antilles to monitor magmatic activity at the surface.

1.2 Interest of muon tomography

Muon radiography was recently successfully used to image the density structure of volcanoes (Tanaka *et al.*, 2005, 2007a, b, 2008; Tanaka and Yokoyama, 2008). This technique measures the flux of muons of cosmic origin and its attenuation due to the screening by the rock volume. The attenuation is directly related to the quantity of matter (expressed in kg m^{-2}) encountered by the muons along their path across the volcano. Muon radiography consequently constitutes a unique way to obtain direct information on the density distribution of geological objects. In practice, a muon radiograph is obtained by measuring the flux of muons crossing the volcano and arriving at the detector in different horizontal and vertical directions. These directions span the solid angle corresponding to the angular aperture of the telescope.

Knowledge of the density distribution inside a volcano is particularly important in terms of constraining its mechanical behavior in case of flank collapse. For example, a volcano like La Soufrière has been partly damaged by both phreatic explosions, which opened fractures, and by hydrothermal acid fluids, which transformed the original

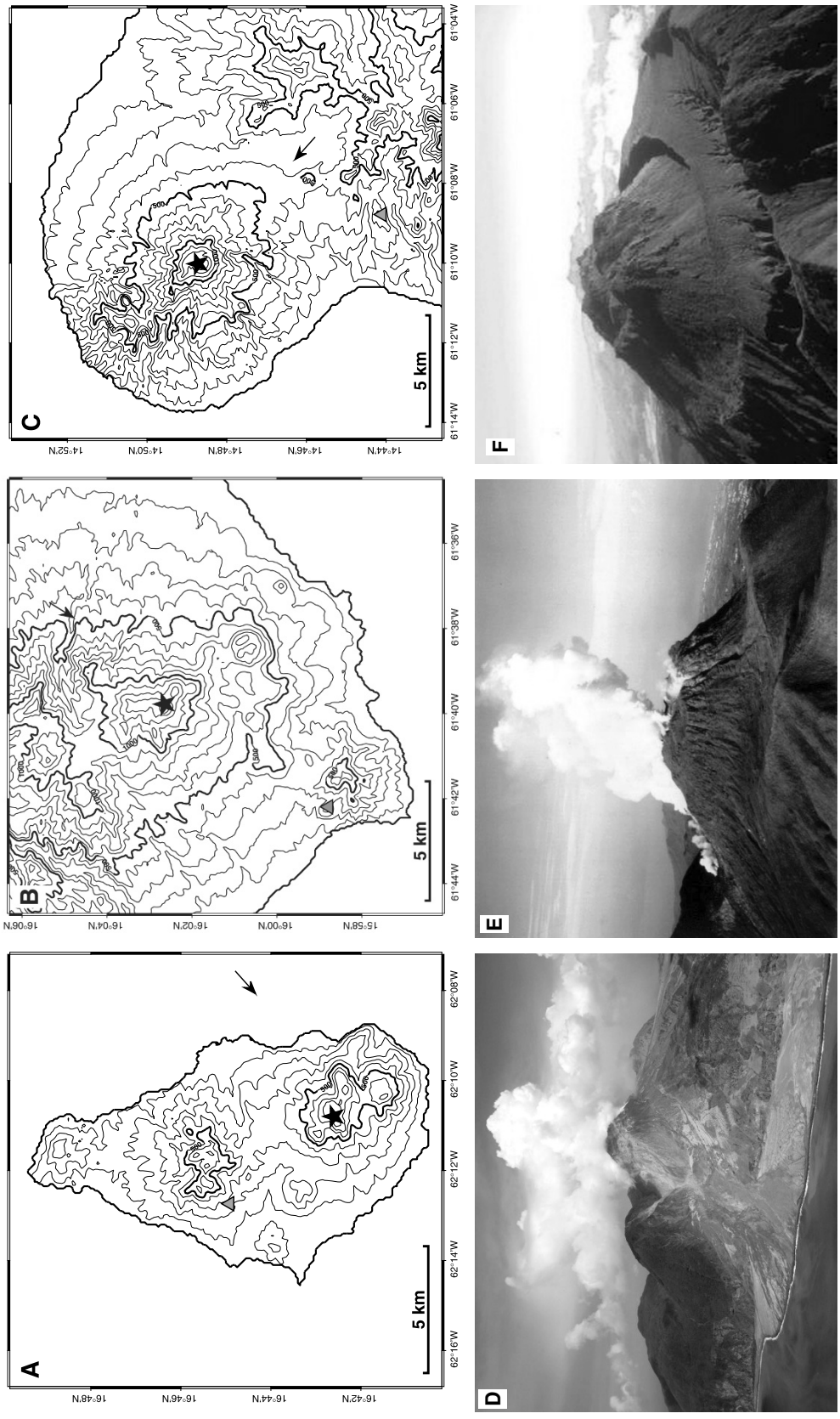

Fig. 2. Location of Lesser Antilles islands with their active volcanoes considered in this paper. A) Montserrat: The Soufrière Hills (D) shown in 2008 and in its current state in a magmatic eruption (http://www.mvo.ms). B) Guadeloupe: La Soufrière (E) shown during its last phreatic eruption in 1976 and its current state in an increasing activity period. C) Martinique: La Montagne Pelée (F) currently in quiet state since its last magmatic eruption in 1929–1932. Black stars indicate lava domes positions. Gray triangles are permanent observatories. Thin arrows indicate approximate view angles of each photograph. Level lines are 100-m intervals (Digital Elevation Model from Shuttle Radar Topography Mission database).

volcanic rocks (andesite, ashes) into hydrothermalized material. Knowing the most affected parts of the volcano is of a primary importance to be able to estimate both the volume of rock potentially involved and the areas exposed in the case of flank destabilization. For this, a global density tomography of the volcano is necessary. Time monitoring is also necessary to follow density variations associated with fluid movements in the volcano and possibly related to liquid/vapour transformation in the shallow hydrothermal system. With respect to volcanoes in a magmatic eruption state like the Soufrière Hills, muon radiography could be an interesting alternative to radar techniques (Wadge *et al.*, 2008) for real-time monitoring of dome growth and eventual collapse. Indeed, muon radiography would be an all-weather operational technique unaffected by the opacity of ash clouds and electrostatic discharges. Also, muon telescopes can be operated in deep caves, a location that provides efficient protection against ash and block fall.

The *DIAPHANE* project was launched at the begining of 2008 to initiate and promote muon tomography in the French Earth Science and Particle Physics communities. The first objectives of the project were to make technological choices for the muon telescopes and to define a design suitable for the difficult field conditions encountered on tropical volcanoes. Telescopes have been constructed and are now being tested. These points are developed in the next sections with a particular emphasis on La Soufrière of Guadeloupe where preliminary field operations have been undertaken to prepare for the installation of the telescopes.

2. Design of Muon Telescopes

2.1 General design and mechanical concept

Several environmental factors make the field condition very difficult on tropical volcanoes such as La Soufrière of Guadeloupe. Heavy rain necessitates careful waterproofing of the telescopes, and rough topography necessitates the use of rope access techniques and helicopter hauling. This puts strong constraints on both the size and the weight of the elements of the telescopes whose design must be modular. A practical rule of thumb is to have each part of the telescope weighing no more than a person, i.e. ≈80 kg so that classical rescue techniques, like Tyrolean systems, operated by a small number of persons can be used to move and install the telescopes. This approach also enables the use of the helicopter winches also designed for rescue operations. The mechanical parts of the telescopes must also be adaptable to the local topography in order to allow an accurate positioning of the detectors with respect to the target of the radiography experiment.

The chosen solution consists of a metallic rigid frame which can be assembled on the field and may receive a variable number of detector matrices with adjustable distance and inclination (Fig. 3) (see chapter 9 in Nagamine, 2003). The frame has adjustable legs that allow a secured adjustment on unequal topography and a precise orientation of the telescope towards the geological target to be tomographied. The waterproofed cases housing the detector matrices are frames with a thickness of 9 cm, and their faces are covered with anodized aluminium plates. This case contains one detector matrix with its associated electronic board and auxiliary sensors for environmental monitoring (temperature, inclination, humidity). A third case contains the on-board computer and the data logger connected to the environmental sensors. All elements must either be resistant to or protected against shocks eventually occurring during helicopter hauling and field installation. This is particularly true for the multianode photomultipliers which, depending on the particular field conditions encountered, may be plugged in at the very end of the telescope installation. The whole system is covered with a robust tarpaulin tightly secured onto the frame and whose role is not only to protect the telescope against heavy tropical rain but also to reduce temperature fluctuations and limit high temperatures of the electronic devices during the rare but nevertheless sunny days that occur.

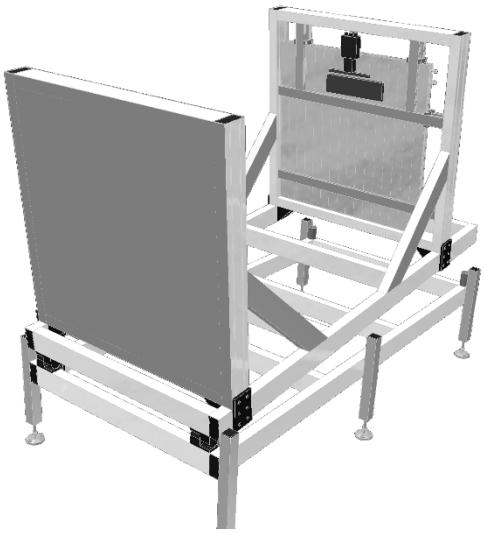

Fig. 3. General view of a telescope configured with two detector matrices. The left matrix is shown with its frame closed as during field operations. The frame of the right matrix is open and the detector matrix (Fig. 4) is visible together with the optical cookie, the photomultiplier, and the electronic boards. The whole system is protected by a tarpaulin not shown on the picture. The frame basis is long enough to allow a distance between the matrices of about 2.5 m, i.e., an aperture angle of 65 for 32×32 matrices and 35 for 16×16 matrices.

2.2 Detection matrices

The detection matrices consist of scintillator bars arranged in two orthogonal series of X rows and Y columns. The number of bars depends on several parameters:

- the detection surface needed to measure a sufficient number of muon trajectories in a reasonable amount of time;
- the weight constraint discussed above;
- the 64 channels permitted by each photomultiplier (PM) and its associated electronic board;
- the desired angular resolution.

The matrices constructed to date are either 16×16 or 32×32 matrices respectively made with $1 \times 5 \times 80\text{-cm}^3$ or $1 \times 5 \times 160\text{-cm}^3$ bars of plastic scintillator (Fig. 4). The matrices then count either 1024 or 256 pixels of $5 \times 5\ \text{cm}^2$ in size. The plastic scintillator bars are produced by the facilities of the Fermi National Accelerator Laboratory (FNAL) (Pla-Dalmau *et al.*, 2001, 2003). The bars used

Fig. 4. View of two 16 × 16 matrices. The optical plugs are visible on two sides of each matrix and are to be connected to the clear bers guiding the light onto the channels of the photomultiplier. The thickness of the matrices is 27 mm and their individual total weight is 20 kg.

in the present study have a cross-section of 1 × 5 cm^2 and have with both a hole for WLS ber insertion and a TiO_2 re ective coating. Bars of 160 cm in length were delivered by FNAL to construct the 32 × 32 matrices. Some of these bars were cut to assemble the 16 × 16 matrices. The weight of a 32 × 32 matrix is ≈70 kg and that for a 16 × 16 matrix is ≈20 kg.

The WLS and clear bers are of the type Bicron BCF-91A MC and BCF-98 MC, respectively, both with a diameter of 1 mm. The WLS bers are inserted into the central duct running along the center of the bars. In order to increase the photo-electron yield, the bers are glued along their whole length with the BC-600 optical cement. A re ecting coating is placed at the free end of the ber in order to further increase the yield (Pla-Dalmau *et al.*, 2005). The other end of the WLS ber is connected to optical connectors embedded in the scintillator bar. The connectors have been specially designed to either ensure the coupling of the WLS bers with the clear bers which transmit the green light to the cookie receiving the PM or to receive solid-state silicon photomultipliers for future replacement of the presently used multianode photomultipliers. When a muon hits the detector matrix, the X and Y bars whose intersection forms the pixel crossed by the particle emit UV light which is in turn captured by their WLS bers inserted in their duct. The visible green light produced by the WLS ber is transmitted to a clear ber connected to a channel of the PM.

A cookie is a box with 64 clear bers connecting the clear bers coming from the bars to the pixels of the PM. The box bers can be arranged in an arbitrary way to optically decouple neighbor pixels of the detection matrix. In practice, this is achieved by connecting bers of neighbor pixels of the detector matrix to non-adjacent pixels of the PM. By this way, cross-talk among neighbor channels of the PM cannot be confounded with pixel excitation due to electron showers hitting cluster of pixels on the detector matrix. The grid of scintillator bars forming a detector matrix is covered with sheets of anodized aluminum in order prevent any entry of polluting light (Fig. 4). The bars are glued together to constitute a self-supporting rigid board to be placed in a waterproofed case, as described above.

2.3 Data acquisition system

The acquisition system connected to the detection matrices is composed of 64-channel Hamamatsu H8804-MOD5 photomultipliers plugged into a front-end board connected to an acquisition board speci cally developed for the OPERA experiment (Detection of Neutrino oscillation between CERN and Gran Sasso) (Girerd *et al.*, 2000; PATENT, 2006).

The H8804 devices have a time resolution of 25 ns, and a wavelength range 300–650 nm for a peak wavelength λ = 420 nm. In a multi-anode PM like the H8804, cross-talk may be due to two causes: (1) the light emerges from the bers with an opening angle of about 30° and may hit the wrong cathode, (2) the collection ef ciency of the dynodes is less than 100% and electrons can leak to neighboring dynodes. In both cases, the shuf ing optical box described above, while not suppressing cross-talk, allows it to be to recognized and lters out wrong events.

The front-end board is based on a 32-channel readout device designed by the LAL-IN2P3 laboratory at Orsay, France. The chips comprise 32 front-end channels with individual inputs, trigger, and charge measurement. Each channel includes a variable gain, an auto-trigger channel followed by a comparator, and a charge measurement channel with a track and hold structure. The logical OR of all the comparator outputs gives the trigger. The threshold is global for the 32 channels, and a mask register allows disablement of a noisy channel. The readout of the 32 channels is made through an analog multiplexor in a serial way.

The acquisition board has been designed for the OPERA experiment as a compact acquisition system that includes all the functions necessary to control and read the signal generated by a multi-anode PM. An important advantage of this system is its simplicity of installation, which only requires a PC and a power supply. The board is entirely controlled through an ethernet network with a LINUX operating system running the acquisition software, based on the CORBA (Common Object Request Broker Architecture, www.corba.org) environment. The readout part of the acquisition board includes a 12-bit A/D converter, and the serial analog multiplexor can be read at 5 MHz max. The total readout of the 64 channels takes about 13 μs. A LED pulser is used to drive two LEDs for calibration and test purposes.

2.4 Power and data transmission

Important issues to consider for eld telescopes are power consumption and wireless data transmission. These are of a primary importance on volcanoes like La Soufrière where access to places chosen to install the telescopes are remote from roads and power lines. These eld conditions imply that solar panels coupled with buffering accumulators must be used to produce electrical energy (Fig. 5). Owing to the night/day sequence and to the cloudy conditions prevailing on tropical volcanoes, the effective ef ciency of the solar panels is about 10%, and the energy budget must be carefully evaluated to prevent any power failure while keeping the total weight as small as possible. Note that motorized tracking systems sometimes used to optimize the light collection on the solar panels are not necessary in tropical areas where the Sun's trajectory does not change much be-

Fig. 5. Example of power and transmission equipment for the permanent station *Sanner* operating at the summit of La Soufrière in Guadeloupe. The solar panels have a nominal power of 378 W for a power consumption of 20 W. The buffer accumulators have a capacity of 300 A h. No power failure has ever occurred at this station during 8 years of continuous operation.

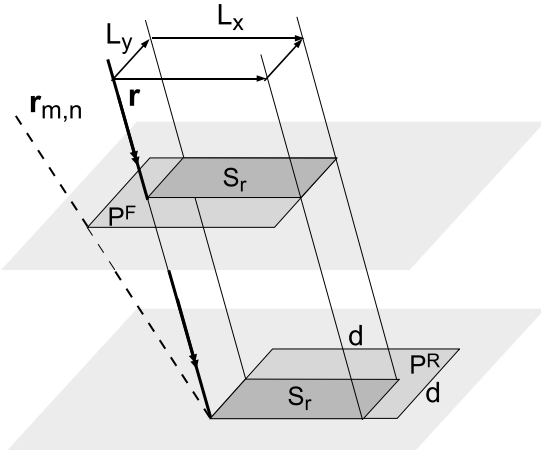

Fig. 6. Detection characteristics of a pair of pixels: P^{F} is a pixel in the front matrix and P^{R} is in the rear matrix. The trajectory with the direction $\mathbf{r}$ is acceptable in the whole rectangular area $S_{\mathbf{r}}$ with sides L_x and L_y. The dashed line represents the direction $\mathbf{r}_{m,n}$ with the largest acceptable area equal to d^2. This direction is the one assigned to all events detected for this pair of pixels.

tween Winter and Summer. Furthermore, such mechanical systems are vulnerable devices under warm and humid atmospheric conditions. For Montserrat, implementation of the telescopes fuel cells should include in the equipment in order to prevent power failure due to ash fall on the solar panels.

Power consumption is divided among the acquisition boards (8 W each), the radio link (4 W), and the on-board computer (15 W). This amounts to a total power of about 35 W for a telescope composed of two 32×32 detector matrices and, depending on the exact location of the telescope, to about 200–350 W of solar panels. A pack of buffer accumulators of 500 A h is necessary for a complete week without solar panel charging in case of very cloudy weather as might occur during the cyclonic period.

Real-time data transmission is desirable for several reasons. Because of the high probability of telescope damage due to the aggressive environment (heavy rain, wind, volcanic acid gases, local landslides,...) it is preferable to remotely collect the data to eliminate the risk of losing several weeks of data records. Also, real-time acquisition of the information provided by the environmental sensors is necessary to check that the telescope is operating normally. We use 5 GHz WiFi communication systems for both their bandwidth capacity and their transmission capabilities over a distance of 10–20 km, a sufficient range in most cases. For instance, the distance between La Soufrière and the volcanological observatory in Guadeloupe is about 9 km. The rough topography around the volcano often necessitates using relay WiFi stations because the observatory is not in the line of sight of the telescope. This problem is particularly true for muon radiography where the telescopes must be placed at low-altitude points around the volcano.

3. Resolution and Tomography Inversion

3.1 Resolution of detector matrices

In contrast to emulsions for which the solid angle, Δ, defining the total aperture of the telescope is spanned continuously (at least theoretically) (Tanaka *et al.*, 2007b, c), the use of detector matrices formed with a limited number of pixels of finite size produces a quantization of Δ. This quantization depends on the number of pixels $N_x \times N_y$, on their size d, and on the distance, D, separating the two detector matrices. In the following discussion, we shall neglect the thickness of the scintillator bars which should, ideally, be considered.

The main cause for angular quantization is that a given pair of pixels, $\{P^{\mathrm{F}}_{i,j}, P^{\mathrm{R}}_{k,l}\}$, of the front and the rear matrix, respectively, may be fired by muons whose trajectory $\mathbf{r}$ belongs to a small solid angle centered on a direction $\mathbf{r}_{i,j,k,l}$ which will be assigned to all muons whatever their actual trajectories (Fig. 6). All pairs of pixels $\{P^{\mathrm{F}}_{i,j}, P^{\mathrm{R}}_{k,l}\}$ with the same relative position $\{m = i - k, n = j - l\}$ have the same common direction which may be written $\mathbf{r}_{m,n}$. Consequently, a telescope made with two matrices counting $N_x \times N_y$ pixels each will have $(2N_x - 1) \times (2N_y - 1)$ discrete directions $\mathbf{r}$ spanning the solid angle Δ. For instance, the 32×32 matrices described in the preceding section will have 3969 discrete directions.

The direction $\mathbf{r}_{0,0}$ is normal to the detector matrices and corresponds to the $N_{0,0} = N_x \times N_y$ pairs of homolog pixels $\{P^{\mathrm{F}}_{i,j}, P^{\mathrm{R}}_{i,j}\}$. For $\mathbf{r}_{m,n}$ with $\{m, n\} \neq \{0, 0\}$, $N_{m,n} < N_{0,0}$ and, the larger the shifts $|m|$ and $|n|$, the smaller $N_{m,n}$. This indicates that the directions near $\mathbf{r}_{0,0}$ will benefit from a large detection area (i.e., number of pairs of pixels), while those too far from $\mathbf{r}_{0,0}$ will have a negligible detection area and will be practically useless. All trajectories detectable by a given pair of pixels have a corresponding detection area, noted $S_{\mathbf{r}}$ in Fig. 6. By projecting $S_{\mathbf{r}}$ perpendicularly to $\mathbf{r}$ and integrating over all acceptable directions, we obtain the detection surface $S_{m,n}$ (in cm^2 sr) of the pair of pixels. Summing over the $N_{m,n}$ pairs associated with $\mathbf{r}_{m,n}$, we obtain the total detection area $\Sigma_{m,n}$.

Figure 7 shows the angular aperture for two matrices with $N_x = N_y = 32$, $d = 5$ cm, and $D = 100$ cm. The aperture of the detection system slightly exceeds $\pm 50^\circ$, as can be seen on the X and Y axes of the figure. The angular

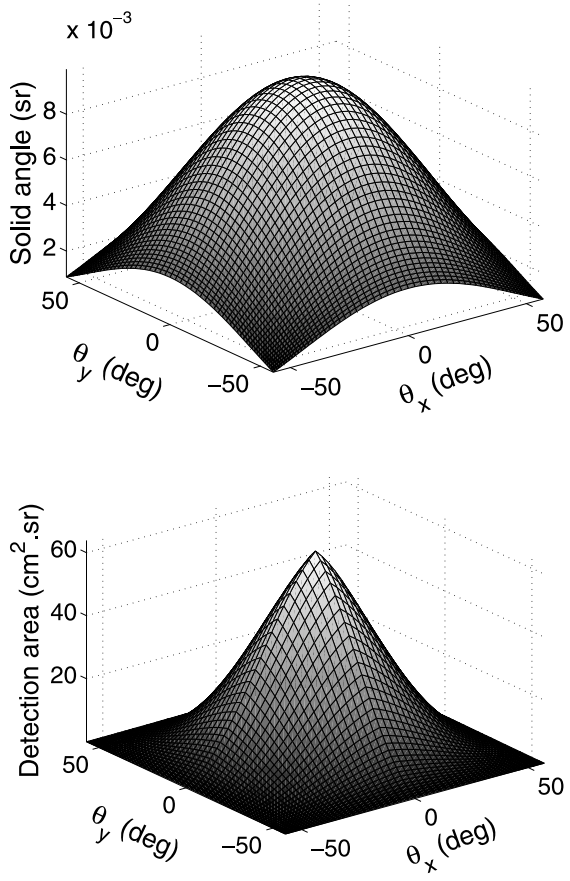

Fig. 7. Azimuthal angular properties of a telescope with two 32×32 matrices located 1 m apart. Top: Angular resolution for each discrete angle of sight of the pair of matrices. Bottom: Integrated detection surface $\Sigma_{m,n}$ for each discrete angle of sight.

aperture for each $\mathbf{r}_{m,n}$ is shown in the top part of Fig. 7. As expected, the poorest angular resolution is obtained for the $\mathbf{r}_{0,0}$ direction normal to the matrices. The detection area $\Sigma_{m,n}$ is shown in the bottom part of Fig. 7. The largest detection surface reaches $\simeq$60 cm^2 sr and is obtained for the normal direction $\mathbf{r}_{0,0}$. $\Sigma_{m,n}$ is almost zero for a margin corresponding to the directions which most depart from $\mathbf{r}_{0,0}$. This is understandable by recalling that for these extreme directions, the pixel pairs have both a smaller angular aperture (see top part of Fig. 7) and a strong obliquity effect which reduces the size of the projected area of the pixels. For the example shown in Fig. 7 we can observe that the effective angular aperture of the telescope is restricted to a cone of $\pm 20^\circ$ around $\mathbf{r}_{0,0}$.

3.2 Simulation of measurements

The detection characteristics computed in the preceding section can now be used to estimate the flux of muons collected by a telescope. A first estimate can roughly be determined by using a crude flux value of 1.5×10^{-6} # cm^{-2} sr^{-1} s^{-1}, which corresponds to about 500 m of rock screening (Nagamine, 2003). Multiplying this flux with a typical detection surface $\Sigma \simeq 30$ cm^2 sr, we get a number of events of about 4 # day^{-1} for each direction $\mathbf{r}_{m,n}$. Several tens of days will be necessary to obtain the number of events necessary to reach a good signal-to-noise ratio. This, of course, depends on the actual thickness of rocks crossed by the muons and on both the location and orientation of the telescope, which may influence the number of perturbing backward events.

3.3 Remarks about the tomography inversion

The tomography inversion aims at reconstructing the 3D density distribution, $\rho(\mathbf{u})$, inside the volcano based on a collection of measurements of the flux of muons after their passage across the rock volume. This problem presents some similarity with the classical X-ray computed tomography encountered in medical imaging. However, the muon tomography problem differs from basic X-ray tomography in several aspects, which we now briefly present.

The flux measurements provide information on the integrated density (expressed in kg m^{-2}),

$$\mathcal{I}_{\mathcal{R}_v}(\rho) = \int_{\mathcal{R}_v} \rho(\mathbf{u})\, \mathrm{d}l, \tag{1}$$

for a collection of paths $\mathcal{R}_v$ along which the density is integrated.

The most basic transmission tomography problem is the so-called parallel-geometry configuration where the paths $\mathcal{R}_v$ are parallel straight lines with direction $\mathbf{n}$ and densely filling the volume to be imaged. To obtain a complete data set allowing a unique recovery of ρ, the number of directions $\mathbf{n}$ must satisfy the *Orlov* condition (Orlov, 1975). Among the many acquisition geometries satisfying this condition, a simple one is when the direction of projection $\mathbf{n}$ spans all directions in a plane, i.e., $\mathbf{n} = \cos\alpha.\mathbf{n}_1 + \sin\alpha.\mathbf{n}_2$ with $0 \leq \alpha \leq \pi$ and where $\mathbf{n}_1$ and $\mathbf{n}_2$ are orthogonal unit vectors. In such a case, the data constitute an ensemble of 2D Radon transforms (sometimes called the X-ray 3D Radon transform) of the density distribution, and ρ is reconstructed through inverse Radon transforms (Bracewell, 2000).

Because of the point-like geometry of the telescopes relative to the size of a volcano, the integration paths $\mathcal{R}_v$ are not parallel lines but instead have a conical geometry, as shown in Fig. 8. The resulting conical tomography may be made equivalent to the parallel tomography described above and involves the first derivative of the Radon transform of the object (Grangeat, 1991). For this, the data set must satisfy the *Tuy* condition (Tuy, 1983). Note that this condition is not satisfied if the acquisition point (i.e., the telescope) describes a full circle around the volcano.

Neither the *Orlov* nor the *Tuy* conditions can be satisfied for measurements performed on a volcano, and the tomography reconstruction will practically be performed with a hugely incomplete data set. This makes the inverse tomography problem very ill-posed with a non-uniqueness of the solution and eventually fully unresolved parameters (Tarantola, 2005). The inverse problem may be made more tractable by using additional information provided either by other geophysical tomography models (electrical, seismic, mechanical) or by prior geological data. Also, the tomography inversion can be made more stable by carefully choosing the parametrization of the model, i.e., the way by which the density distribution ρ is mathematically represented (e.g., Tarantola and Nercessian, 1984).

The particular points mentioned above reveal the complicated nature of the inverse problem in muon tomography.

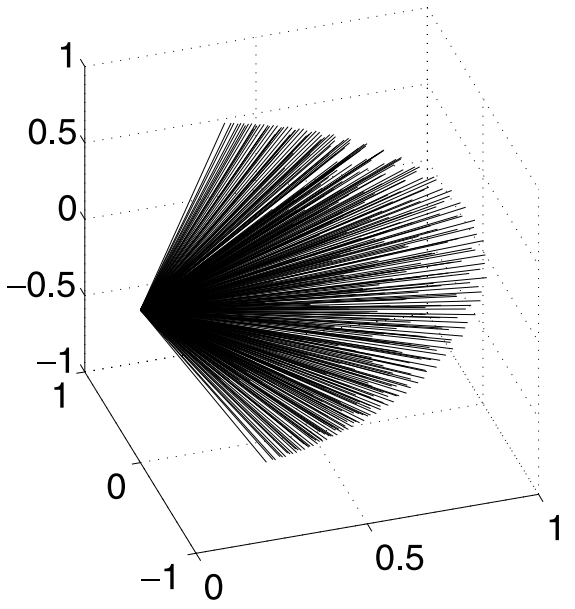

Fig. 8. Figure showing the conical-like geometry to the directions of detection for a telescope with two 32 × 32 matrices located 1 m apart.

Without any claim for exhaustiveness, let us cite several difficulties which augment this complexity. The stochastic and imprecise nature of the forward problem giving both the flux of incident muons and their interaction with matter should ideally be considered in a probabilistic framework (Tarantola, 2005). The finite angular resolution of each detection direction $\mathbf{r}_{m,n}$ implies that the integration (1) is not actually done along a mathematical line but, instead, in a conical volume with a square cross-section. This situation is already considered in other geophysical tomography problems, like seismic imaging where the Fresnel zone is sometimes used instead of the "line-like" asymptotic rays (e.g., Dahlen *et al.*, 2000; Dahlen and Baig, 2002).

4. Examples of Field Implementations

Although muon tomography is planned for the three volcanoes presented above, we shall only discuss the example of La Soufrière on Guadeloupe, which shall host the first tomography experiments.

4.1 Present status and geophysical survey of La Soufrière on Guadeloupe

For about 17 years, La Soufrière on Guadeloupe volcano is showing significant signs of unrest, monitored by the permanent observatory. The present unrest episode started with a renewal of volcanic seismicity in 1992, with a first seismic swarm associated with reactivation of the previously extinct Cratere Sud fumarole, the appearance of a new warm-spring at the south base of the dome (Pas du Roy), and reactivation of the Tarade warm-spring south of the dome. Overall, the seismic activity was characterized by shallow-depth (up to 3 km deep), low-energy events located below the lava dome (see Fig. 9) and irregular time variations in the number of events, energy released, and felt earthquakes, as well as several generally prolonged seismic swarms superimposed to a higher than normal base level seismicity. These events are probably evidence of micro-fracturation of very altered and thus mechanically weak host-rocks by the superficial hydrothermal system due hydrothermal fluids heated by a variable heat and gas flux coming from the deeper magma reservoir but without injections of magma to shallow depths (Komorowski *et al.*, 2005). Other reactivations of fumaroles occurred in 1996 (Napoleon crater), 2000 (Tarissan Pit), and 2007 (1956 Pit), while the Cratere Sud slowly increased in gas flux, gas temperatures (up to 140°C), and spatial extent of the thermal anomaly. In 1998, the sudden apparition of chlorine in the fumaroles at Cratere Sud led to an increase of acidity of the gas (pH below zero) that is still present. This general trend is confirmed by monitoring the boiling acid-lake discovered in 2002 in the bottom of Tarissan Pit (about 80 m below the surface).

The changes observed on this volcano also motivated a number of geophysical experiments aimed at providing an insight into the present inner structure of the lava dome and at following and quantifying its presently ongoing evolution. Several of these geophysical experiments give us a view of the structure of the entire dome.

A complete set of electrical resistivity data acquired on and around the dome reveals that the lava dome is very heterogeneous and composed of blocks of either almost unaltered massive lava or of hydrothermalized and unconsolidated products of various type (clays, granular media) (Nicollin *et al.*, 2006). Figures 10 and 11 summarize the information on the geo-electrical structure of the dome. Figure 10 shows the results of geo-electrical sounding inversions where the colored cylinders represent vertical conductivity profiles inverted with data acquired at different locations on and around the lava dome. The electrical conductivity varies over a wide range (notice the $\log_{10}$ color scale in the figure) due the highly heterogeneous structure of the dome. In particular, regions of high conductivity (i.e., purple and blue on the figure) are observed at the base of the dome and correspond to a layer of hydrothermalized materials (Nicollin *et al.*, 2006). This layer is inclined in the southwest direction, which corresponds to the main direction of potential flank destabilizations (Le Friant *et al.*, 2006; Komorowski *et al.*, 2008). Figure 11 shows a slice in the geo-electrical structure which reveals the deep conductive zones corresponding to hydrothermalized volumes of rock and their connection with the hydrothermal active zone at the summit. Other geo-electrical experiments like "mise-à-la-masse" measurements (e.g., Parasnis, 1967) have shown that the deep part of the dome is occupied by a wide conductive zone connected to the acid lake of the Tarissan pit. This conductive zone probably corresponds to a shallow hydrothermal reservoir filled with hot concentrated acid.

The "blocky" structure of the dome can also be observed with mechanical tomography which relies on the deformation data acquired on the main faults and fractures of the dome (Jacob *et al.*, 2005). Preliminary results from seismic tomography further confirm a dome structure as a juxtaposition of high- and low-velocity domains (O. Coutant, pers. comm.). All tomography methods applied up to now indicate that the lava dome of La Soufrière is very heterogeneous with highly-contrasted physical properties, either electrical conductivity or elastic wave velocities. This makes the inversion of the corresponding data particularly

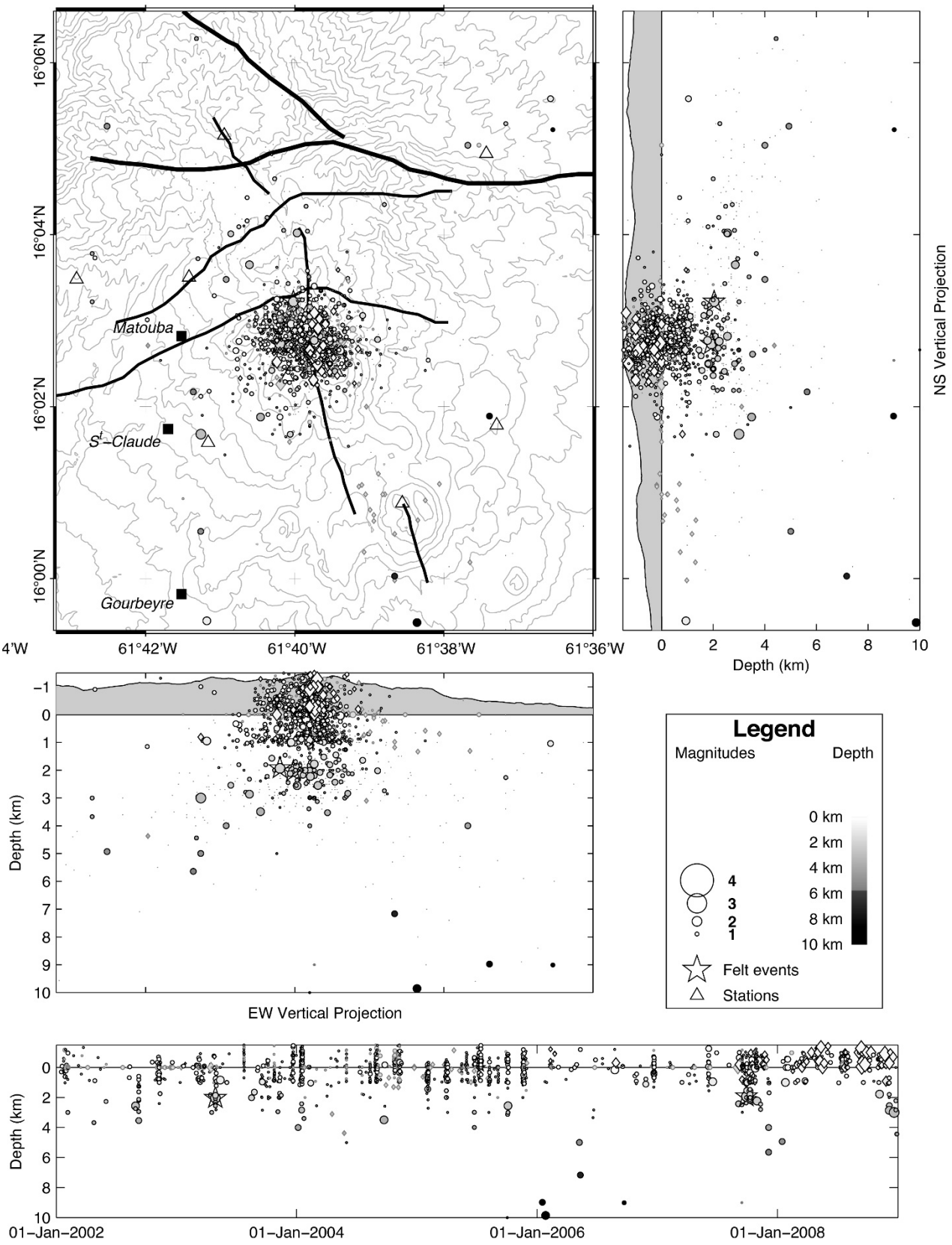

Fig. 9. Volcanic seismic events recorded at Soufrière (Guadeloupe) from 2001 to 2008. Symbols stand for hypocenter locations, size for magnitudes, gray tunes for depth (see inset legend for details). A star around a symbol means a felt event. Circles are volcano-tectonic type events, diamonds are long-period events (no magnitude available). Thick black lines represent main geological structures: regional faults and caldera rims (after Feuillet *et al.*, 2002). Triangles indicate permanent seismic stations. Data and plot modi ed from OVSG-IPGP WebObs monitoring system (Beauducel *et al.*, 2004).

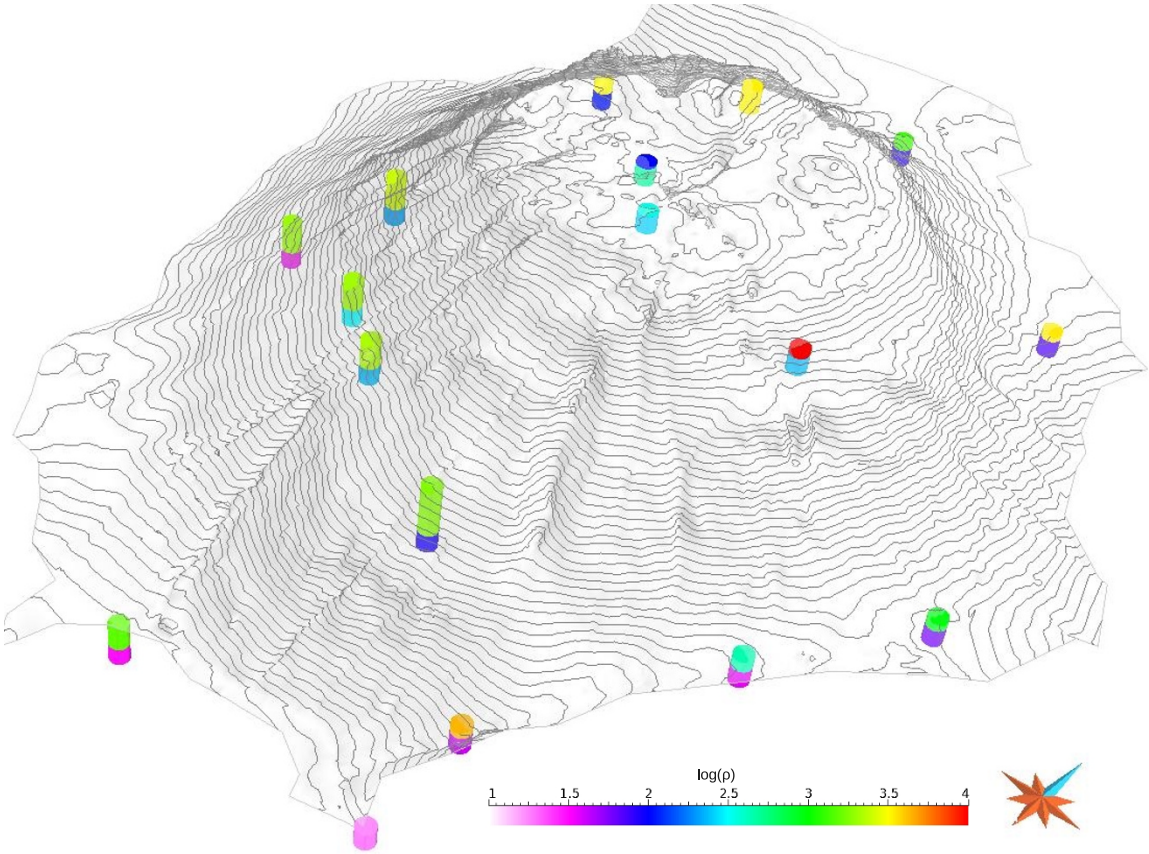

Fig. 10. View of La Soufrière lava dome from the south-east. The colored cylinders represent the results of geo-electrical sounding inversions (Nicollin *et al*., 2006) performed at different locations on and around the dome. These soundings reveal that the dome is highly heterogeneous with the electrically conducting part corresponding to hydrothermalized materials.

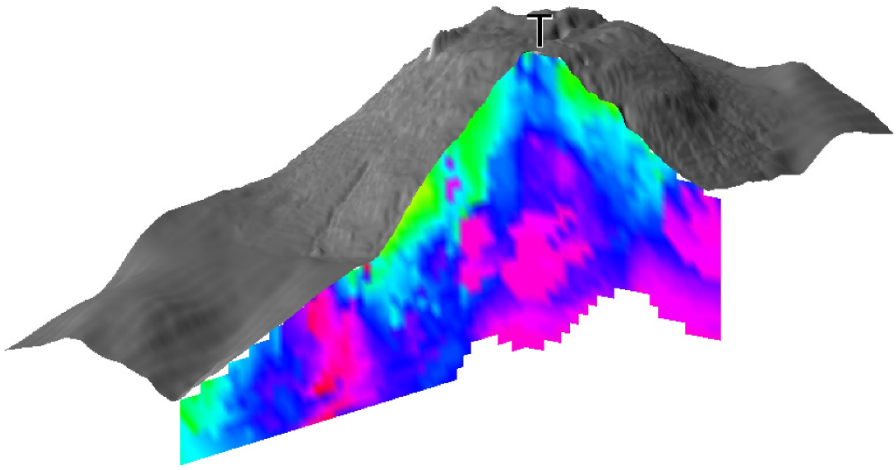

Fig. 11. Cross-sectional view of the geo-electrical structure of La Soufrière lava dome obtained from the pseudo-sections of electrical resistivity from Nicollin *et al*. (2006). The low-resistivity zones are shown in blue and violet. The T letter marks the location of the Tarissan pit.

difficult due to, for instance, strong ray bending in seismic tomography or electrical short-circuits caused by the conductive parts of the volcano. In light of these difficulties, muon tomography is particularly interesting for both the relative simplicity of the inverse problem (i.e., straight rays) and the possibility to focus the telescopes on particular parts of the dome where other geophysical methods are "blind".

The reawakening of several fumarolic areas at the summit of the lava dome also led us to complete the range of techniques used to follow the time-evolution of geophysical and geochemical parameters of these vents. For instance, a regular sampling of the boiling acid lake located in the Tarissan pit has been carried out and, recently, a continuous monitoring of its temperature and level has been implemented to characterize its mass transfer and energy budgets. Despite the huge difficulties encountered in operating

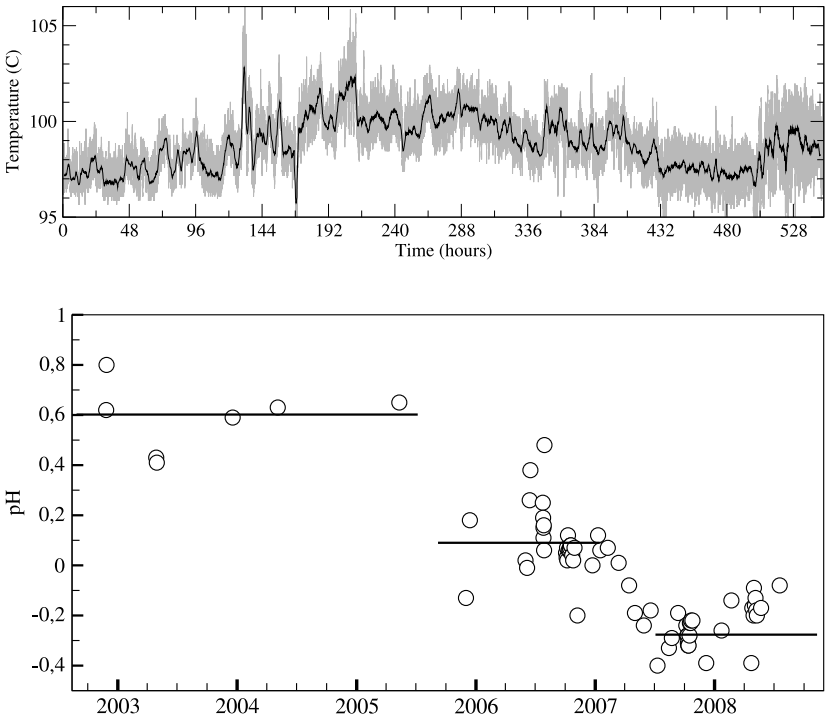

Fig. 12. Top: Time evolution of the temperature in the acid lake of the Tarissan pit. Observe the transient increases of temperature which may be due to fluctuations of the gas flux. Bottom: Time evolution of the pH in the boiling lake in the Tarissan pit. Observe the step-like nature of the evolution curve, which may be produced by gas release in the magma chamber.

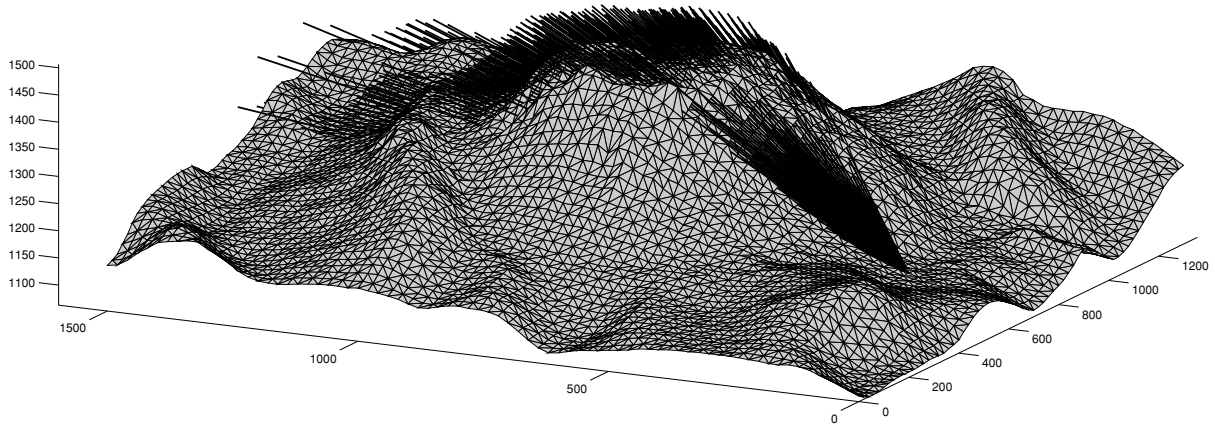

Fig. 13. Simulation of a muon radiography experiment on La Soufrière on Guadeloupe performed with a telescope equipped with two 16×16 matrices located 1 m apart. The point marks the location of the telescope, and the straight black lines represent the discrete lines of sight of the detection system.

these equipments, the data collected up to now clearly show abrupt changes in the physical (Fig. 12 top) and chemical (Fig. 12 bottom) parameters of the shallow hydrothermal system. The causes of the observed changes remain puzzling and may involve a release of both thermal energy and magmatic gases after the fracturing of the plastic envelope surrounding the magma chamber (Fournier, 2007). Alternatively, the opening of channels enabling new exchanges between up-to-now separated hydrothermal reservoirs might also explain the abrupt changes observed. In either case, a precise knowledge of the structure of the lava dome is desirable to help to "deconvolve" the signals emitted by the deep hydrothermal system from shallow effects like channeling, mixing, etc.

For a detailed account of the evolution of the chemical parameters, the reader is referred to the monthly reports of the Volcanological Observatory on the web site of the *Institut de Physique du Globe de Paris*.

4.2 Muon tomography of La Soufrière on Guadeloupe

The prominent situation of the lava dome of La Soufrière (Fig. 2(E)) is particularly convenient for muon tomography, and several places exist where the telescopes can be placed

at the very bottom of the dome (Fig. 13). Also, because the average slope of the dome anks is steep, it is possible to place the telescopes beneath the dome itself, i.e., at a small distance from the rock mass. A further advantage of the prominent topography of La Soufrière is that most of the landscape around the volcano is clear from high nearby mountains that may cause shadows on the muon radiography images.

The proximity between the dome and the telescopes results in a reduction of the ux of atmospheric electrons and positrons which produce false events forming the background noise. The low altitude of the telescope locations relative to the dome implies that, in most situations, the detector planes must be inclined in order to point upward in the direction of the lava dome. Consequently, the backward ux will be mostly ltered out since only backward muons with a nearly horizontal trajectory will be detected by all detector planes.

5. Conclusion

Muon tomography is a novel geophysical imaging method able to provide unique information on the density distribution inside geological volumes with a typical size of 1 km. This method may usefully be applied to study volcanoes, either to provide information on their internal structure or to monitor density changes eventually produced by magma ascent or phase changes occurring in their super- cial hydrothermal reservoirs. Thanks to recent progress made in particle physics, compact and ef cient solutions now exist to design and construct portable telescopes which can be operated under the dif cult eld conditions encountered on tropical volcanoes.

Acknowledgments. The authors thank Paolo Strolin for his ef - cient and kind organization of the Mu-Ray workshop in Napoli. The project bene tted from fruitful discussions with Hiroyuki Tanaka from ERI, Anna Pla-Dalmau and Alan Bross from FNAL, Elvis Dzamastagic from Hamamatsu France Corporation, Dario Autiero and Bruno Carlus from IPNL, Karim Mahiouz from IPGP, and Bruno Kergosien and Pascal Rolland from Géosciences Rennes. The *DIAPHANE* project was initiated with funds provided by the Scienti c Council of the *Institut de Physique du Globe de Paris* and is also nancially supported by ANR RiskNat (*DomoScan* project) for the 2009–2011 period. The data on La Soufrière on Guadeloupe have been kindly provided by the Volcanological and Seismological Observatory of Guadeloupe (http://www.ipgp.fr). This is IPGP contribution number 2591.

References

Baxter, P. J., R. Boyle, P. Cole, A. Neri, R. Spence, and G. Zuccaro, The impacts of pyroclastic surges on buildings at the eruption of the Soufrière Hills volcano, Montserrat, *Bull. Volcanol.*, **67**, 293–313, doi:10.1007/s00445-004-0365-7, 2005.

Beauducel, F., C. Anténor-Habazac, and D. Mallarino, WEBOBS: Integrated monitoring system interface for volcano observatories, *IAVCEI General Assembly, Pucon, Chile, Nov. 2004*, poster & abstract, 2004.

Boudon, G., J.-C. Komorowski, B. Villemant, and M. P. Semet, A new scenario for the last magmatic eruption of La Soufrière of Guadeloupe (Lesser Antilles) in 1530 A.D. Evidence from stratigraphy radiocarbon dating and magmatic evolution of erupted products, *J. Volcanol. Geotherm. Res.*, doi:10.1016/j.jvolgeores.2008.03.006, 2008.

Bracewell, R. N., *The Fourier Transform and Its Applications*, 640 pp., Mc-Graw Hill, New York, 2000.

Dahlen, F. A. and A. M. Baig, Fréchet kernels for body-wave amplitudes, *Geophys. J. Int.*, **150**, 440–466, 2002.

Dahlen, F. A., S.-H. Hung, and G. Nolet, Fréchet kernels for nite-frequency travel-times: I. Theory, *Geophys. J. Int.*, **141**, 157–174, 2000.

Druitt, T. H. and B. P. Kokelaar (eds), The Eruption of Soufrière Hills Volcano, Montserrat, from 1995 to 1999, *Geological Society*, 645 pp, London Memoir 21, 2002.

Elsworth, D., G. Mattioli, J. Taron, B. Voight, and R. Herd, Implications of magma transfer between multiple reservoirs on eruption cycling, *Science*, **322**, 246–248, doi:10.1126/science.1161297, 2008.

Feuillard, M., J. C. Allègre, G. Brandeis, R. Gaulon, J. L. Le Mouël, J. C. Mercier, J. P. Pozzi, and M. P. Semet, The 1975–1977 crisis of La Soufrière de Guadeloupe (F.W.I.): A still-born magmatic eruption, *J. Volcanol. Geotherm. Res.*, **16**, 317–334, 1983.

Feuillet, N., I. Manighetti, P. Tapponnier, and E. Jacques, Arc parallel extension and localization of volcanic complexes in Guadeloupe, Lesser Antilles, *J. Geophys. Res.*, **107**, 2331, 2002.

Fournier, R. O., Hydrothermal systems and volcano geochemistry, in *Volcano Deformation: Geodetic Monitoring Techniques*, edited by D. Dzurisin, Springer, Berlin, 2007.

Girerd, C., S. Gardien, J. Burch, S. Katsanevas, and J. Marteau, Ethernet network-based DAQ and smart sensors for the OPERA long-baseline neutrino experiment, *Nuclear Science Symposium Conference Record, 2000 IEEE*, **2**, 12/111–12/115, 2000.

Grangeat, P., Mathematical framework of cone-beam 3D reconstruction via the rst derivative of the Radon transform, in *Mathematical Methods in Tomography (Lecture Notes in Mathematics)*, edited by Herman, G. T., A. K. Louis, and F. Natterer, 268 pp, Springer, Berlin, 1991.

Herd, R. A., M. Edmonds, and V. A. Bass, Catastrophic lava dome failure at Soufrière Hills Volcano, Montserrat, 12–13 July 2003, *J. Volcanol. Geotherm. Res.*, **148**, 234–252, doi:10.1016/j.jvolgeores.2005.05.003, 2005.

Institut de Physique du Globe de Paris, Bilan mensuel de l'activité volcanique de la Soufrière de Guadeloupe et de la sismicité régionale, *Observatoire Volcanologique et Sismologique de Guadeloupe—IPGP*, ISSN 1622-4523, http://www.ipgp.jussieu.fr/pages/0303040901.php.

Jacob, T., F. Beauducel, G. Hammouya, J. G. David, and J.-C. Komorowski, Ten years of extensometry at Soufrière of Guadeloupe: New constraints on the hydrothermal system, *Paper presented at Soufriere Hills Volcano—Ten Years On international workshop*, Seismic Research Unit, University of West Indies, July 24–30, 2005.

Jolivet, J., La crise volcanique de 1956 à la Soufrière de Guadeloupe, *Ann. Géophys.*, **14**(3), 305–322, 1958.

Komorowski, J.-C., G. Boudon, M. Semet, F. Beauducel, C. Anténor-Habazac, S. Bazin, and G. Hammouya, Guadeloupe, in *Volcanic Atlas of the Lesser Antilles*, edited by J. M. Lindsay, S. Ali, R. E. A. Robertson, J. B. Shepherd, and L. John, 65–102, University of the West Indies, Seismic Research Unit, Trinidad, and IAVCEI, 2005.

Komorowski, J. C., Y. Legendre, B. Caron, and G. Boudon, Reconstruction and analysis of sub-plinian tephra dispersal during the 1530 A.D. Soufrière (Guadeloupe) eruption: Implications for scenario de nition and hazards assessment, *J. Volcanol. Geotherm. Res.*, **178**(3), 491–515, 2008.

Lacroix, A., La Montagne Pelée et ses éruptions, *Masson*, 662 pp, Paris, 1904.

Le Friant, A., G. Boudon, J.-C. Komorowski, P. Heinrich, and M. P. Semet, Potential ank-collapse of Soufrière Volcano, Guadeloupe, Lesser Antilles? Numerical simulation and hazards, *Nat. Haz.*, **39**, 381–393, 2006.

Le Guern, F., A. Bernard, and R. M. Chevrier, Soufrière of Guadeloupe 1976-1977: Eruption-mass and energy transfer and volcanic health hazards, *Bull. Volcanol.*, **43**(3), 577–593, 1980.

Lindsay, J. M., R. E. A. Robertson, J. B. Shepherd, and S. Ali (eds), *Volcanic Hazard Atlas of the Lesser Antilles*, Seismic Research Unit, The University of the West Indies, Trinidad and Tobago, W. I., 279 pp., 2005.

Nagamine, K., *Introductory Muon Science*, 208 pp, Cambridge University Press, Cambridge, UK, 2003.

Nicollin, F., D. Gibert, F. Beauducel, G. Boudon, and J.-C. Komorowski, Electrical tomography of La Soufrière of Guadeloupe Volcano: Field experiments, 1D inversion and qualitative interpretation, *Earth Planet. Sci. Lett.*, **244**, 709–724, 2006.

Orlov, S. S., Theory of three-dimensional reconstruction: 1—Condition of a complete set of projections, *Sov. Phys. Cristallogr.*, **20**, 312–314, 1975.

Parasnis, D. S., Three-dimensional electric mise–la-masse survey of an irregular lead-zinc copper deposit in central Sweden, *Geophys. Prospect.*, **15**, 407–437, 1967.

PATENT, Installation de capteurs intelligents pour l'acquisition à haut débit de données *via* le réseau Ethernet, Patent # 04 00468 (delivered

with number # 06/16 dated 2006.04.21), 2006.

Pla-Dalmau, A., A. D. Bross, and K. L. Mellott, Low-cost extruded plastic scintillator, *Nucl. Instr. Meth.*, **A466**, 482–491, 2001.

Pla-Dalmau, A., A. D. Bross, and V. V. Rykalin, Extruding plastic scintillator at Fermilab, FERMILAB-CONF-03-318, *Proceedings of the 2003 IEEE Nuclear Science Symposium and Medical Imaging Conference*, Portland, Oregon, USA October 16–26, 2003.

Pla-Dalmau, A., A. D. Bross, V. V. Rykalin, and B. M. Wood, Extruded plastic scintillator for MINERvA, FERMILAB-CONF-05-506, *Proceedings of the 2005 IEEE Nuclear Science Symposium and Medical Imaging Conference*, Puerto Rico, October 23–29, 2005.

Romer, M., La dernière Éruption de la montagne Pelée, *Bull. Volcanol.*, **3:4**, 89–116, 1931.

Tanaka, H. K. M. and I. Yokoyama, Muon radiography and deformation analysis of the lava dome formed by the 1944 eruption of Usu, Hokkaido—Contact between high-energy physics and volcano physics, *Proc. Jpn. Acad.*, **B84** 107–116, 2008.

Tanaka, H., K. Nagamine, S. N. Nakamura, and K. Ishida, Radiographic measurements of the internal structure of Mt. West Iwate with near horizontal cosmic ray muons and future developments, *Nucl. Instr. Meth. Phys. Res.*, **A555**, 164–172, 2005.

Tanaka, H. K. M., T. Nakano, S. Takahashi, J. Yoshida, H. Ohshima, T. Maekawa, H. Watanabe, and K. Niwa, Imaging the conduit size of the dome with cosmic ray muons: The structure beneath Showa Shinzan Lava Dome, Japan, *Geophys. Res. Lett.*, **34**, L22311, doi:10.1029/2007GL031389, 2007a.

Tanaka, H., T. Nakano, S. Takahashi, J. Yoshida, M. Takeo, J. Oikawa, T. Ohminato, Y. Aoki, E. Koyama, H. Tsuji, and K. Niwa, High resolution imaging in the inhomogeneous crust with cosmic ray muon radiography: The density structure below the volcanic crater oor of Mt. Asama, Japan, *Earth Planet. Sci. Lett.*, **263**, 104–113, 2007b.

Tanaka, H. K. M., T. Nakano, S. Takahashi, J. Yoshida, and K. Niwa, Development of an emulsion imaging system for cosmic-ray muon radiography to explore the internal structure of a volcano, Mt. Asama, *Nucl. Instr. Meth. Phys. Res.*, **A575**, 489–497, 2007c.

Tanaka, H. K. M., T. Nakano, S. Takahashi, J. Yoshida, M. Takeo, J. Oikawa, T. Ohminato, Y. Aoki, E. Koyama, H. Tsuji, H. Ohshima, T. Maekawa, H. Watanabe, and K. Niwa, Radiographic imaging below a volcanic crater oor with cosmic-ray muons, *Am. J. Sci.*, **308**, 843–850, 2008.

Tarantola, A., *Inverse Problem Theory and Methods for Model Parameter Estimation*, 342 pp., Society for Industrial and Applied Mathematics, Philadelphia, 2005.

Tarantola, A. and A. Nercessian, Three-dimensional inversion without blocks, *Geophys. J. R. Astron. Soc.*, **76**, 299–306, 1984.

Tuy, H. H., An inversion formula for cone-beam reconstruction, *SIAM J. Appl. Math.*, **43**, 546–552, 1983.

Villemant, B., G. Hammouya, A. Michel, M. P. Semet, J.-C. Komorowski, G. Boudon, and J.-L. Cheminée, The memory of volcanic waters: shallow magma degassing revealed by halogen monitoring in thermal springs of La Soufrière volcano (Guadeloupe, Lesser Antilles), *Earth Planet. Sci. Lett.*, **237**, 710–728, 2005.

Wadge, G., D. G. Macfarlane, H. M. Odbert, M. R. James, J. K. Hole, G. Ryan, V. Bass, S. De Angelis, H. Pinkerton, D. A. Robertson, and S. C. Loughlin, Lava dome growth and mass wasting measured by a time series of ground-based radar and seismicity observations, *J. Geophys. Res.*, **113**, doi:10.1029/2007JB005466, 2008.

D. Gibert (e-mail: gibert@ipgp.fr), F. Beauducel, Y. Déclais, N. Lesparre, J. Marteau, F. Nicollin, and A. Tarantola